Indian Journal of Engineering & Materials Sciences
Vol. 27, February 2020, pp. 77-86

Investigation of the effective parameters on welding residual stress in GTAW of aluminum cylindrical shell

Yousef Ghaderi Dehkordi[a], Ali Pourkamali Anaraki[a*] & Amir Reza Shahani[b]

[a] Department of Mechanical Engineering, Shahid Rajaee Teacher Training University, Tehran 16758 136, Iran

[b] Faculty of Mechanical Engineering , K.N. Toosi University of Technology, Tehran 16765 3381, Iran

Received:27 August 2018; Accepted:22 August 2019

The present work aims to study the influence of different geometrical, technological, and material parameters on residual stress in tungsten inert gas butt-welded aluminum cylinder. In order to present a simple analytical model to estimate the welding residual stress, the Taguchi L18 array has been employed with one 6-level factor and four 3-level factors. A 3D coupled thermo-mechanical finite element model considering temperature-dependent material properties has been developed to determine the welding residual stress in all experiments. The numerical model has been validated using the hole-drilling method. Using statistical analysis, the order of factors based on their effect on residual stress has been determined as yield strength, length, thickness, heat input, and finally diameter. The residual stress increases with an increase in yield strength, diameter, and heat input, while decreases with an increase in thickness. Contribution of each parameter on residual stress has been specified using variance analysis; yield strength with 99.6% contribution is the most significant factor, while diameter has insignificant impact. Finally, high accuracy equations have been proposed to calculate the welding residual stress.

Keywords: Welding residual stress, Finite element, Experimental design, Taguchi, Aluminum, Cylindrical shell

1 Introduction

Welding technology is widely used in production, maintenance and repair of structures. However, the high-localized heating and subsequent cooling lead to generation of tensile residual stress near to the weld line, which has adverse effect on performance of the welded components[1-3]. Therefore, an accurate evaluation of the welding residual stress is essential to assess the safety and tolerability of structures. During the past years, numerical methods based on the finite element (FE) analysis have been developed to simulate the welding process. For example, the FE technique was used to study the residual stress and distortion fields in welded aluminum stiffened plates [4], butt-welded Monel plates[5], combined butt and fillet weld joint of steel plates[6], welded steel stiffened plates[7], and welded pipe joint of dissimilar steels[8]. Xu *et al.*[9] studied the effect of metal strength on the residual stress in steel welded joins based on the experimental measurement and FE simulation. Pandey *et al.*[10] developed a 3D FE analysis to study the effect of welding direction on residual deformation and temperature history in the submerged arc welding of double-sided fillet joints. They conducted the experimental measurements to verify the numerical results successfully. Pandey *et al.*[11] also used the FE method to study the effect of diffusible hydrogen in deposited metal in multipass welded steels. Chaurasia *et al.*[12] studied the residual stresses of different welding methods experimentally. They measured the residual stresses of friction stir welding and tungsten inert gas (TIG) welding in welded steel plates using the hole-drilling method. It was observed that the magnitude of longitudinal residual stress of TIG welded joints was higher than friction stir welded joint. Javadi *et al.*[13] investigated the clamping effect on welding residual stress of stainless steel plates by using the ultrasonic stress measurement method and FE analysis. They concluded that using the clamp significantly influences the deformation and the residual stress fields in the base metal. Ye *et al.*[14] studied the influences of weld groove type on residual stress in a butt-welded joint by means of numerical simulation and experiment. It was concluded that the groove shape has a significant influence on welding residual stress. Pandey *et al.*[15] evaluated the effect of grove design and number of welding pass on the transverse residual stress in the TIG welding of P91 steel pipes. They showed that the shrinkage stress in the narrow groove is less than that of the conventional

*Corresponding author (E-mail: ali_pourkamali@sru.ac.ir)

V-groove. Similar results were reported by Giri *et al.*[16]. Pandey *et al.*[17] reviewed the microstructure evolution and the mechanical properties of welded P91 steel pipes in different heat treatment condition. It was demonstrated that to obtain the desired properties and microstructure, it is necessary to perform the proper heat treatment after welding[18-20]. They also reported that re-austenitizing based tempering produced uniform microstructure and hardness across the weld joints in the TIG welding of dissimilar P91 and P92 steels[21]. The thermo-mechanical elastic plastic FE method cannot be used to calculate welding deformation of large and complex welded structures due to the limitation of computing speed. Hence, Vishvesha *et al.*[22] used the elastic FE method based on the inherent strain theory to predict distortion in a welded ring of the guide blade carrier of a steam turbine. Several studies have been conducted to investigate the effects of process variables such as the heat input parameters[23, 24] and welding sequence[25] on welding residual stress of steel alloys.

According to the literature, it is clear that despite the vast research on welding simulation, there has been no analytical model to predict the influence of effective parameters on welding residual stress, especially for welded cylindrical shells of the work-hardened aluminum of 5000-Series. Further, experimental design is a beneficial method to identify the effective parameters and their impacts on the response variable. In this paper, experimental design is conducted to study the influence of various effective parameters on residual stress in axially welded aluminum cylinders. It is worth pointing out the axial weld in thin cylindrical vessels is a critical joint where the damage often initiated. Here, thickness, diameter, and length of the cylinder were selected as the geometrical parameter, heat input was selected as the technological parameters, and the yield strength of the base material was chosen as the material parameter. In order to provide a new simple analytical model, the Taguchi L18 array is employed with one 6-level factor and four 3-level factors. First, a 3D thermo elasto-plastic FE model, considering temperature-dependent material properties and a moving volumetric heat source, is developed to determine the welding residual stress in experiments, by the ABAQUS software. The FE model is successfully validated by the experimental measurement of stresses. Using statistical analysis, the order of factors based on their effect on welding residual stress is determined as the yield strength, length, thickness, heat input, and finally diameter. In addition, the residual stress increases with an increase in the yield strength, diameter, and heat input, while decreases with an increase in the thickness. Further, contribution of each parameter on the welding residual stress is determined using variance analysis. Finally, high accuracy equations are proposed that can be used to calculate the welding residual stress in terms of design factors.

2 Experimental Procedure

In order to verify the FE analysis, the residual stresses on the outside surface of the axially welded cylinder were measured using the experimental method.

2.1 Material and specimen preparation

The experimental specimen was prepared through axial welding of a cylindrical shell with diameter 800 mm, length 500 mm, and thickness 2 mm. The material is a non-heat-treatable aluminum of 5000-Series that is strengthened through cold-working process. The alloy has excellent corrosion resistance, moderately high strength, and good welding qualities without the necessity for post-weld treatment[26]. This alloy commonly used in the manufacture of high strength welded structures, pressure vessels, marine components, and storage tanks. The optical emission spectroscopy was utilized to determine the chemical composition of the alloy and the results are given in Table 1. The thermo-physical properties of the material are shown in Fig. 1[27].

The welding process is the gas tungsten arc welding (GTAW) that used the non-consumable electrode made of pure tungsten and the high purity (99.99%) argon as shielding gas. The single-pass welding was done by automatic welding machine with the process

Table 1 — Chemical composition of the investigated aluminum.

Element	Al	Mg	Ti	Zn	Mn	Cu	Fe	Si
%	92.52	6.36	0.048	0.074	0.648	0.026	0.181	0.161
Element	Cr	Sb	Be	Zr	B	Sn	Pb	Ni
%	0.005	0.003	0.0006	0.003	0.0008	0.002	0.006	0.006

parameters given in Table 2. These values were selected according to a prequalified welding procedure specifications, in which the range of current is 140-180 A, range of gas flow rate is 10-15 L/Min, and the power supply will maintain the user selected current by automatically adjusting the voltage supplied (constant current mode). During welding, the specimens were restricted at the top with two clamps at a distance of 16 mm from the weld centerline. Due to the high effect of yield strength on welding residual stress, the mechanical specifications of the material were obtained in elevated temperatures by high-temperature tensile test, based on the ASTM E 21 standard[28], as shown in Fig. 2. The specimen geometry and the prepared specimens, which were exploited for this test, are shown in Fig. 3.

2.2 Residual stress measurement

Over the years, several methods have been developed to measure the welding residual stress in different types of components[29]. The hole-drilling method is the most widely used technique for measuring the residual stresses. It offers advantages of good accuracy and reliability, standardized test procedure, non-significant damage, and convenient practical implementation[30]. In this study, this method was utilized to measure the welding residual stresses. For strain measurement, five strain gauges of type delta rosette were attached to the top surface of the specimen after welding as shown in Fig.4.

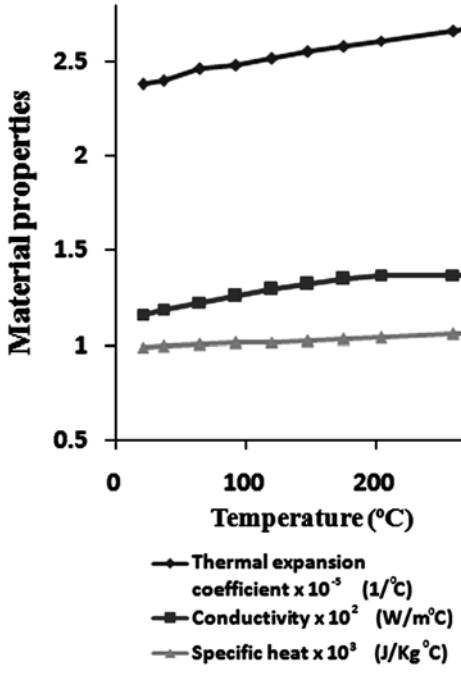

Fig. 1 — Thermal properties of the materials versus temperature.

Table 2 — Parameters of the welding procedure.

Current-AC (A)	Voltage (V)	Speed (cm/Min)	Shielded gas	Gas flow rate (L/Min)
170	10	9.6	Argon	12

3 Welding Simulation of Axial Butt Weld in the Cylindrical Shell

3.1 General considerations

A 3D FE model was developed in ABAQUS software, using the element birth technique based on

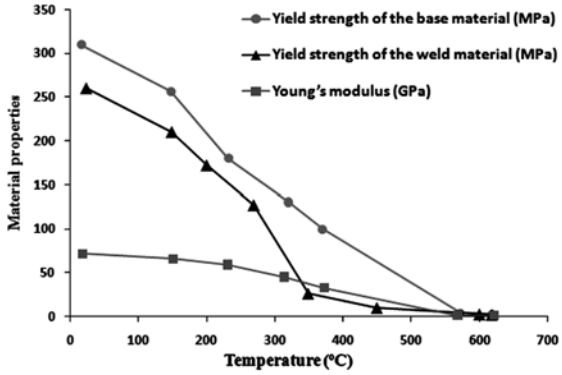

Fig. 2 — Mechanical properties of the materials versus temperature.

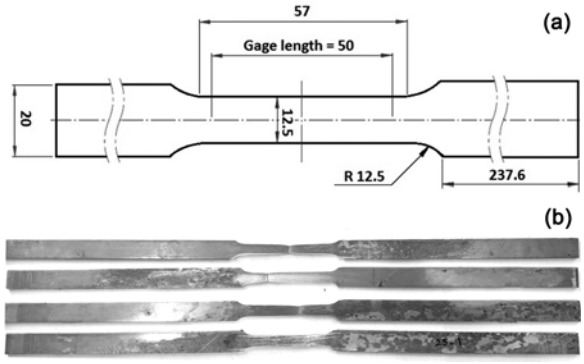

Fig. 3 — (a) Specimen geometry and (b) prepared specimen used for high temperature tensile test.

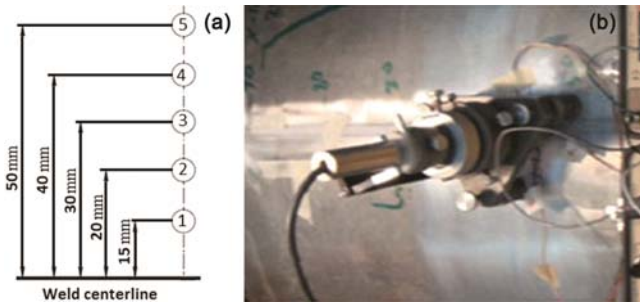

Fig. 4 — Welding residual stress measurement (a) gauge positions and (b) hole drilling machine.

the thermo-mechanical couple method. In this method, the temperature history was determined by the thermal analysis, and the subsequent mechanical analysis was performed by applying the predicted temperatures as the initial load. The analysis is composed of three stages as presented in Table 3. In the thermal analysis, the heat transfer element DC3D20 was employed, and in the mechanical analysis, the reduced integration element C3D20R was used. The thermal gradient is larger at the welding zone, so the finer mesh size was applied near the weld line as shown in Fig. 5. In order to reduce computation time, half symmetry condition was applied in the FE model. For the boundary condition, the restrictions due to the clamps of welding machine should be considered. Therefore, the nodes of the elements at distance 16 mm away from the weld centerline were clamped during welding process, and then released due to removing the clamps. The effect of mesh size, was investigated for four FE models as shown in Fig. 6. Based on the method proposed by Malik *et al.*[31], the peak temperature was selected as the investigated parameter in the mesh sensitivity analysis. It is clear that the temperature is independent of the mesh size beyond 16000 elements. Therefore, the model No. 3 was selected for the further analysis.

Table 3 — Stages of the FE analysis.

Stage number	Stage time (s)	Stage specification
Stage 1	312.5	Heating (welding time)
Stage 2	2500	Cooling
Stage 3	1	Releasing the clamps

3.2. Thermal analysis

The Goldak's model[32] was used for the heat source modelling as illustrated schematically in Fig. 7. In this model, the heat flux distribution for the front and the

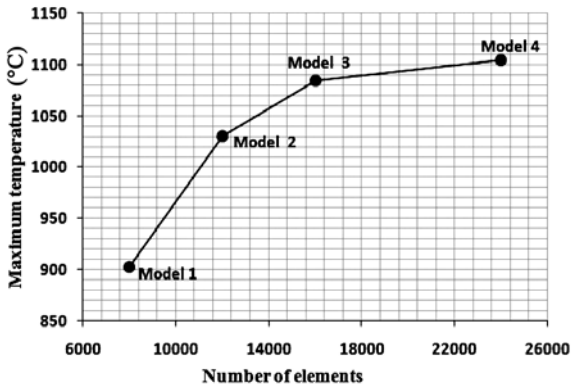

Fig. 6 — Mesh sensitivity analysis in different models.

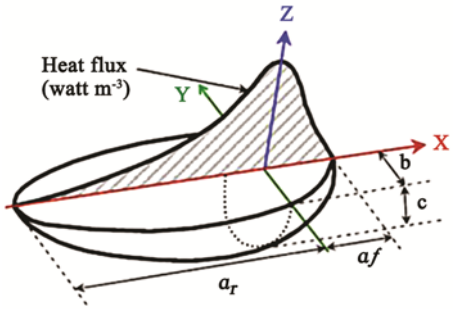

Fig. 7 — Double-ellipsoidal heat source model.

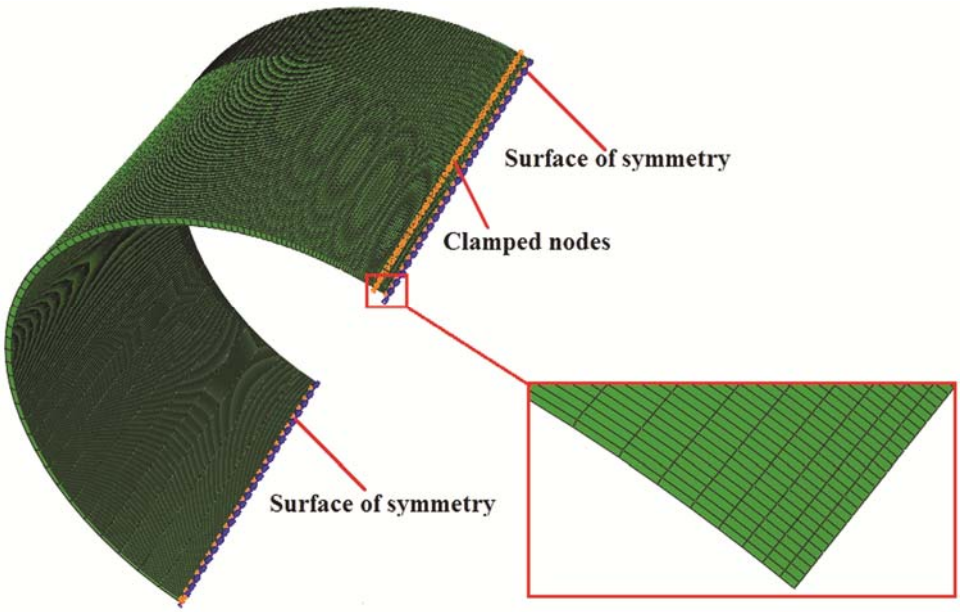

Fig. 5 — FE model for the welding simulation.

rear ellipsoids were presented respectively, as follows:

$$q_f(x,y,z) = \frac{6\sqrt{3}\eta Q f_f}{\pi\sqrt{\pi}a_f bc} exp(-\frac{3x^2}{a_f{}^2} - \frac{3y^2}{b^2} - \frac{3z^2}{c^2}) \quad \ldots (1)$$

$$q_r(x,y,z) = \frac{6\sqrt{3}\eta Q f_r}{\pi\sqrt{\pi}a_r bc} exp(-\frac{3x^2}{a_r{}^2} - \frac{3y^2}{b^2} - \frac{3z^2}{c^2}) \quad \ldots (2)$$

where, a_f, a_r, b, and c are the dimensional constants of the Goldak's model, parameter Q is the total heat power, and parameter η is the thermal efficiency which is assumed to be 70% for the TIG welding[33]. The parameters f_f and f_r are the heat fraction coefficients in the front and the rear ellipsoids, respectively, where $f_f + f_r = 2$[32]. Here, a_f, a_r, b, and c are considered 4, 12, 4, and 2 mm, respectively and f_f and f_r are 1.5 and 0.5.

In the thermal analysis, to calculate the heat flux within the elements, a user subroutine, namely, DFLUX, is developed. Another subroutine, called FILM, is developed to account for the heat loss coefficient. For simplicity, this coefficient is defined as a combination of convection and radiation coefficients as follow[25]:

$$h_{total} = \left[h_{convection} + \varepsilon\sigma(T + T_{amb})(T^2 + T_{amb}^2)\right] \quad \ldots (3)$$

where, $h_{convection}$ is the convection heat transfer coefficient (8 W/m^2 ℃), ε denotes emissivity (0.2), σ is the Stefan-Boltzman constant (5.67×10^{-8} W/m^2K^4) [25], and T_{amb} is the ambient temperature.

3.3. Mechanical analysis

Total strain rate during welding is decomposed as follow[25]:

$$\dot{\varepsilon_t} = \dot{\varepsilon_e} + \dot{\varepsilon_p} + \dot{\varepsilon_{th}} + \dot{\varepsilon_{pt}} \quad \ldots (4)$$

where, $\dot{\varepsilon_e}$, $\dot{\varepsilon_p}$, $\dot{\varepsilon_{th}}$, and $\dot{\varepsilon_{pt}}$ denote the strain rate components due to elastic, plastic, thermal loading, and phase transformation, respectively. During welding of the 5000-Series aluminum, phase transformation does not occur, so $\dot{\varepsilon_{pt}}$ component is not considered.

3.4. Results and analysis of welding simulation

Fig. 8 shows the predicted temperature history during the welding. The monitoring points 1 and 2 have zero and 8 mm distance from the weld centerline, respectively. It is expected that the monitoring point 1 exhibits the higher temperature compared to the monitoring point 2. As seen, at the time that the heat source intersects the line of monitoring points, the highest temperatures are achieved. The welding temperature histories are specified by a rapid heating, high peak temperature, rapid cooling, and returning to ambient temperature.

Fig. 9 shows the comparison of the axial and the hoop residual stresses of the FE method and the experimental measurement. As seen, the maximum axial residual stress (300 MPa) equals to the yield strength of the shell material approximately. Whereas, the global maximum value of the hoop residual stress

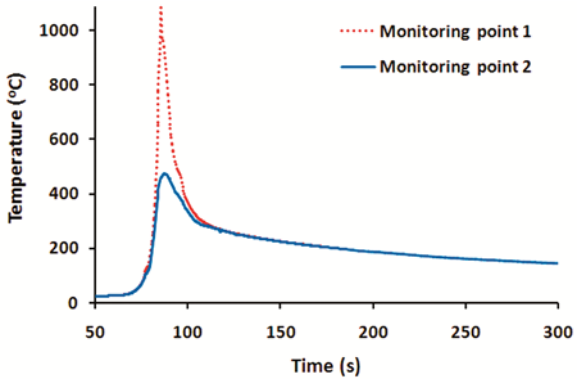

Fig. 8 — Welding temperature history at monitoring points.

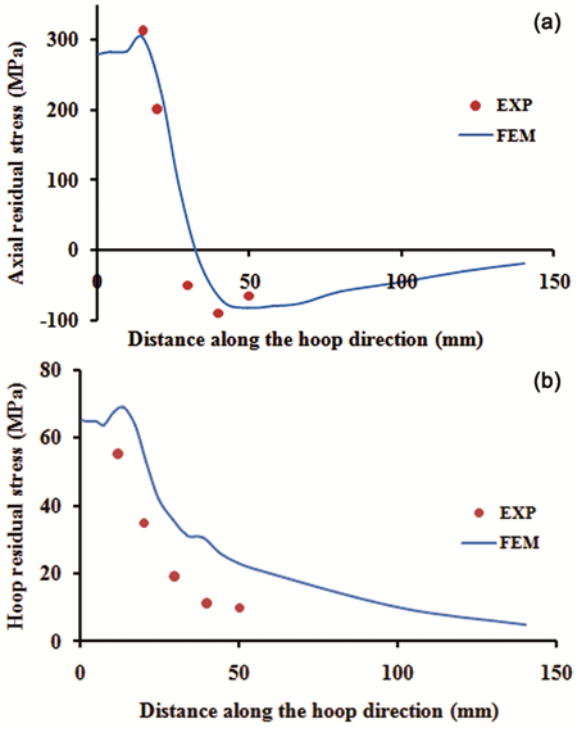

Fig. 9 — (a) Axial and (b) hoop residual stress distributions.

(65 MPa) is much lower than the yield strength. Hence, a good agreement is observed between the FE analysis and the experimental method.

4 Design of Experiments

Since there are many effective factors on the welding analysis, design of experiments using the Taguchi technique[34] was employed to evaluate the effect of main factors on the welding residual stress.

The Taguchi method is an important tool for design of experiments that offers a simple, efficient and systematic approach to optimize designs for performance, quality, and cost. This technique causes a decrease in the number of experiments with no reduction of accuracy from the full factorial method. Its simplicity in data collection, as well as practicality in designing the process parameters, makes design of experiment possible in any product and process optimization. Hence, it is strongly recommended to use this technique in improving the process quality. In the Taguchi approach, the design of experiment process will consider all the main factors and their influence on the response variable. This method presents guidance on which factors are significant to be controlled and which levels are suitable to put quality characteristic on target.[35,36]

Here, thickness (t), diameter (d), and length of the cylinder (l) were selected as the geometrical parameters, heat input (q) was selected as the technological parameter, and the yield strength of the base material (S_y) was chosen as the material parameter. All parameters were studied in three levels, except the thickness, which was investigated in six levels. According to the number of design factors and their levels, the Taguchi's L18 orthogonal array was used in this study to conduct the experiments. The investigated factors and their levels are shown in Table 4. The maximum value of the axial welding residual stress was selected as the response variable. Using the FE analysis, the response variables were determined for all experiments, as compared in Fig. 10.

(I) *Taguchi analysis:* Taguchi analysis was performed and the results are given in Table 5. This table presents the maximum axial residual stress for every level of design parameters. In this table, the Delta parameter is the maximum difference of response variable between the levels of each factor, and the

Table 4 — The design factors and their levels.

Exp. no.	t (mm)	d (mm)	L (mm)	q (W)	S_y (MPa)
1	1	800	500	500	170
2	1	1600	1000	600	240
3	1	2400	1500	700	310
4	2	800	500	600	240
5	2	1600	1000	700	310
6	2	2400	1500	500	170
7	3	800	1000	500	310
8	3	1600	1500	600	170
9	3	2400	500	700	240
10	4	800	1500	700	240
11	4	1600	500	500	310
12	4	2400	1000	600	170
13	5	800	1000	700	170
14	5	1600	1500	500	240
15	5	2400	500	600	310
16	6	800	1500	600	310
17	6	1600	500	700	170
18	6	2400	1000	500	240

Table 5 — Average values of the maximum axial residual stress in every level of each factor (MPa).

Level	t	d	l	q	S_y
1	236.3	234.7	235.7	234.0	166.8
2	235.3	235.3	232.8	236.8	235.0
3	235.3	235.3	236.8	234.5	303.5
4	233.0	-	-	-	-
5	236.7	-	-	-	-
6	234.0	-	-	-	-
Delta	3.7	0.7	4.0	2.8	136.7
Rank	3	5	2	4	1

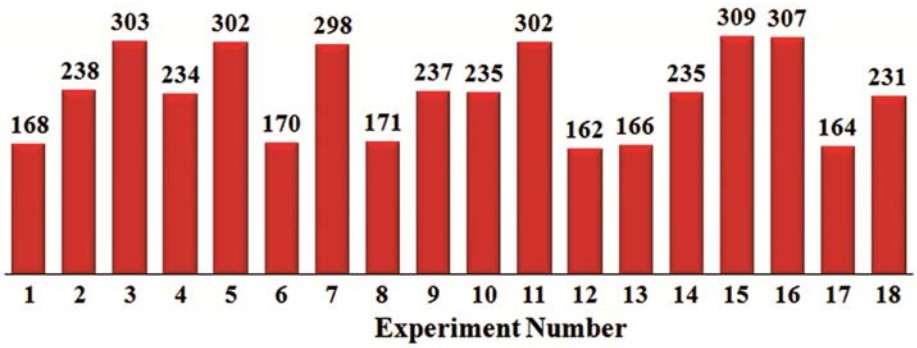

Fig. 10 — Maximum axial residual stress for all experiments (MPa).

Rank parameter specifies the rank of each factor based on the Delta values. As seen, the yield strength and the shell diameter are the two parameters with the most and the least effects, respectively.

This can be also observed in the plot of design factor impacts shown in Fig. 11. As seen, the yield strength affects the response variable significantly; an increase in the yield strength causes the welding residual stress to increase, while the effect of the shell diameter is rather insignificant. As determined from the rank values, the order of factors based on their effect on the axial residual stress is as follows: yield strength, length, thickness, heat input, and finally diameter.

(II) *Regression analysis:* The regression analysis was performed to derive the relationship between the design factors and the response variable. By this method, the maximum value of axial welding residual stress was estimated through the first order regression by Eqs. (5) and (6), as follows:

$$\sigma = 2.48 - 0.286t + 0.00042d + 0.00117l + 0.0025q + 0.9556 \quad \dots (5)$$

$$\sigma = 97.11 - 0.286t + 0.33d + 0.58l + 0.25q + 68.33S_y \quad \dots (6)$$

The above equations actually represent a single relationship with the same result. Eq. (5) is the numerical and Eq. (6) is the encoded forms of the relationship. For instance, for a yield strength of 240 MPa, one should place 240 as S_y in Eq. (5); however, it has to be replaced by 2 in Eq. (6) according to Table 4. The numerical form is proposed for simplicity of calculations, which does not require dividing of the parameters and encoding.

Similar to the first order equations, second order equations were presented in the numerical and the encoded forms; Eq. (7) is the numerical and Eq. (8) is the encoded forms, as follows:

$$\sigma = -90 - 1.08t + 0.00042d - 0.026l + 0.312q + 1.075S_y + 0.113t^2 + 0.000014l^2 - 0.00026q^2 - 0.00025{S_y}^2 \quad \dots (7)$$

$$\sigma = 101.5 - 1.08t + 0.333d - 13.082l + 10.58q + 67.67S_y + 0.113t^2 + 3.42l^2 - 2.58q^2 + 0.17{S_y}^2 \quad \dots (8)$$

In the regression analysis, R^2 is the percentage of variation in the response explained by the model. In this study, the values of R^2 ($R^2 > \%99$) indicate that the fit of the experimental data to the model is satisfactory.

(III) *Analysis of Variance:* The Analysis of Variance (ANOVA) was performed to understand how much change of each variable has contributed, as well as which variable is statistically important. The ANOVA results for the second order regression are shown in Table 6. The sum of squares indicates the relative importance of each factor; the factor with the biggest sum of squares has the greatest impact. The p-value also shows the significance level of each factor; a smaller p-value corresponds to a greater significance. Table 6 indicates that the yield strength (p=0.00), length (p=0.08), thickness (p=0.14), heat input (p=0.63), and diameter (p=0.73) in this order are the most significant factors affecting axial residual stress.

Table 6 — ANOVA results for the axial residual stress.

Source	Sum of squares	p-Value	Contribution
t	27.1	0.14	0.03%
d	1.3	0.73	0.00%
l	41.9	0.08	0.04%
q	2.5	0.63	0.01%
S_y	513.0	0.00	99.61%
t*t	1.4	0.72	0.00%
l*l	46.7	0.07	0.08%
q*q	26.7	0.15	0.05%
S_y*S_y	6.4	0.45	0.03%

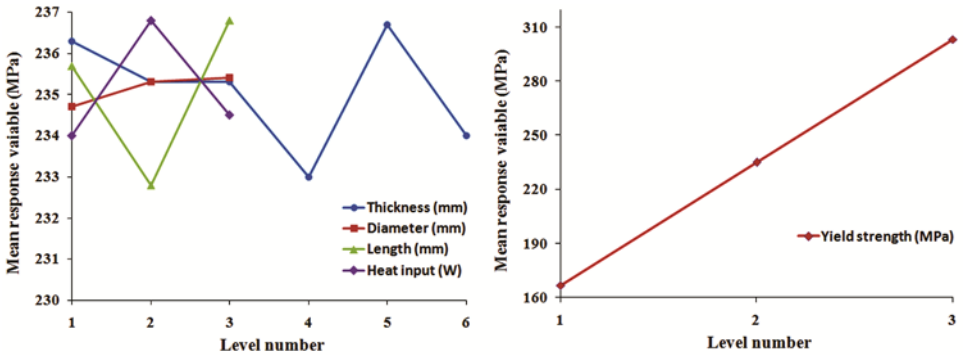

Fig. 11 — Effect of design factors on the axial residual stress.

In addition, the yield strength with 99.6% contribution has the most impact on the axial residual stress. Note that these conclusions are completely compatible with the Taguchi results.

Figures 12 and 13 show the residual plot for the proposed first and second order equations, respectively. This plot is helpful in assessing whether the model satisfies the assumptions of the analysis. The residuals assumed to be random and normally disturbed. Histogram of the residuals indicates that the data is normally disturbed. In addition, the residual versus order plots displays no pattern in data distribution. This proves that the residuals are independent from one another. As seen, the maximum residual value of the second order equation is 4.5, which is acceptably improved compared with the first order equation in which maximum residual value is 6.5.

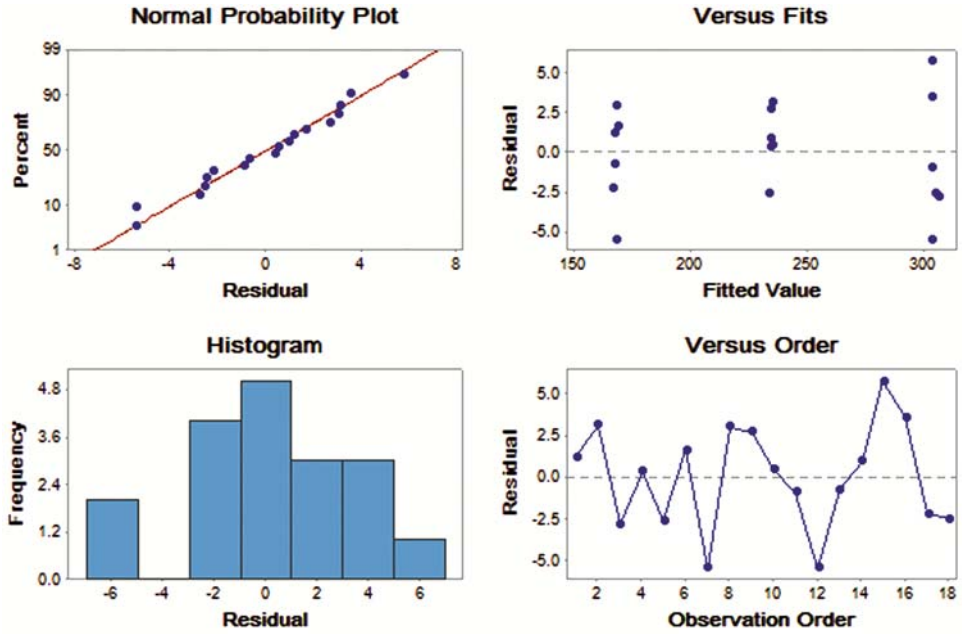

Fig. 12 — Residual plots for the first order equation.

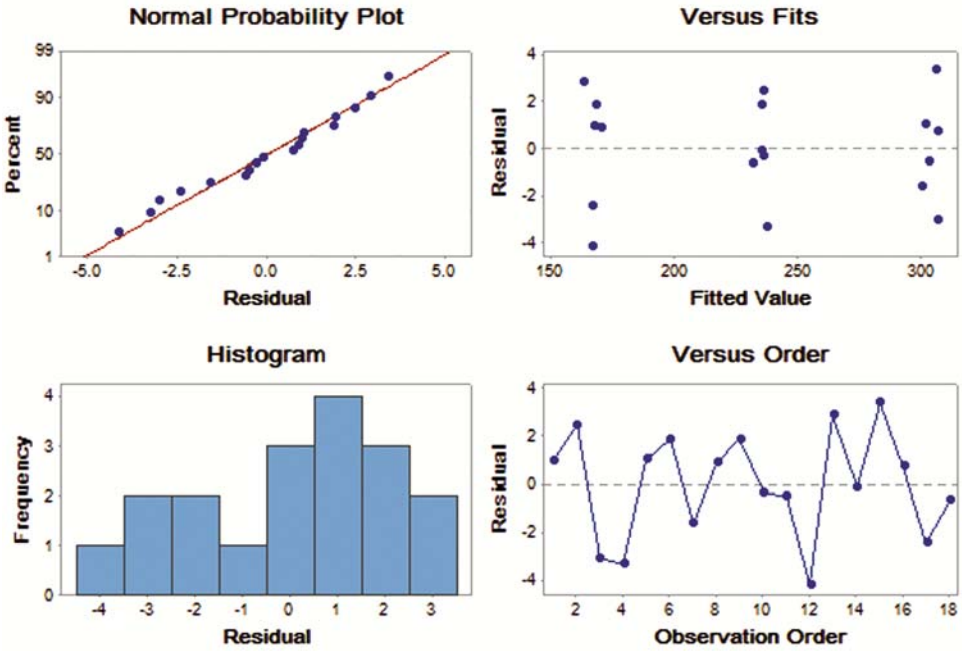

Fig. 13 — Residual plots for the second order equation.

Table 7 — Comparison between the results of FEM and equations (MPa).

Exp. no.	FEM	First order equation		Second order equation	
		Eq. (5)	Difference (%)	Eq. (7)	Difference (%)
1	168	166.8	-0.70	166.8	-0.68
2	238	234.9	-1.31	235.5	-1.03
3	303	305.8	0.93	306.4	1.12
4	234	233.7	-0.14	237.1	1.31
5	302	304.6	0.86	300.9	-0.36
6	170	168.4	-0.96	168.6	-0.83
7	298	303.5	1.84	299.6	0.53
8	171	168.0	-1.75	170.5	-0.26
9	237	234.3	-1.14	234.9	-0.89
10	235	234.5	-0.20	235.7	0.31
11	302	302.9	0.31	302.2	0.08
12	162	167.5	3.37	166.2	2.59
13	166	166.8	0.46	163.1	-1.73
14	235	234.1	-0.40	235.5	0.22
15	309	303.2	-1.86	305.3	-1.19
16	307	303.5	-1.15	306.6	-0.12
17	164	166.2	1.36	166.2	1.36
18	231	233.5	1.10	231.6	0.26

In order to verify the regression analysis, the results of the FE analysis were compared with the equation values as presented in Table 7. As seen, the relative difference of Eqs (5) and (7) are less than 3.37% and 2.59%, respectively, which are related to Experiment 12. This is compatible with the residual plots shown in Figs. 11 and 12.

5 Conclusions

This paper studied the influence of the main effective factors on the welding residual stress in the thin-walled cylinder of work-hardened Aluminum alloy. First, the 3D FE analysis of axial welding of the cylindrical shell was developed for predicting the welding residual stress. To validate the FE simulation, the residual stresses were measured through the hole drilling method. Next, the Taguchi experimental design method was applied to investigate the effect of various geometrical, technological and the material variables on the welding residual stress. In summary, the following conclusions can be drawn:

(1) The developed FE analysis gives accurate results for welding residual stress, so it can be used to obtain the values of response variable in the experimental design.

(2) The yield strength, the cylinder length, the cylinder thickness, the heat input, and the cylinder diameter in this order are the most significant design factors affecting the axial welding residual stress.

(3) The yield strength is recognized as the most important parameter, while the diameter has insignificant impact on the axial residual stress.

(4) The welding residual stress increases with an increase in the yield strength, the diameter, and the heat input and decreases with an increase in the thickness.

(5) The closed form equations are proposed to calculate the axial welding residual stress based on the thickness, diameter, length, heat input, and yield strength, with high accuracy

References

1 Xiu J, Li Y & Cheng Y, *J Adhes Sci Technol*, 32 (2017) 1.
2 Cui C, Zhang Q, Bao Y, Kang J & Bu Y, *J Constr Steel Res*, 148 (2018) 450.
3 Zhang W, Jiang W, Zhao X & Tu S T, *Int J Fatigue*, 109 (2018) 182.
4 Farajkhah V & Liu Y, *Mar Struct*, 50 (2016) 95.
5 Javadi Y, *J Press Vessel Technol*, 137 (2015) 011.
6 Kumanan S & Vaghela S, *Ind J Eng Mater S*, 24 (2017) 201.
7 Chen B Q & Soares C G, *Int J Adv Technol*, 86 (2016) 2723.
8 Xia J & Jin H, *Int J Precis Eng Man*, 19 (2018) 57.
9 Xu M, Chen J, Jin Y, Li Y & Lu H, *Sci Technol Weld Joi*, 20 (2015) 208.
10 Pandey C, Giri A & Mahapatra M M , *Int J Steel Struct,* 16 (2016) 333.
11 Pandey C, Mahapatra M M, Kumar P & Saini N, *Metall and Mater Trans B*, 49 (2018) 2881.
12 Chaurasia P K, Pandey C, Giri A, Saini N & Mahapatra M M, *Arch Metall Mater*, 63 (2017) 1019.
13 Javadi Y, Hasani M & Sadeghi S, *J Non destruct Eval*, 34 (2015) 3.
14 Ye Y, Cai J, Jiang X, Dai D & Deng D, *Adv Eng Softw* 86 (2015) 39.
15 Pandey C, Narang H K, Saini N, Mahapatra M M & Kumar P, *Int J Steel Struct,* 17 (2017) 763.
16 Giri A, Mahapatra M M, Sharma K & Singh P K, *Int J Steel Struct* 17 (2017) 65.
17 Pandey C, Mahapatra M M, Kumar P & Saini N, *J Alloy Compd*, 743 (2018) 332.
18 Pandey C & Mahapatra M M, *J Mater Eng Perform*, 25 (2016) 2195.
19 Pandey C, Mahapatra M M, Kumar P & Kumar S, *J Mater Process Technol*, 266 (2019) 140.
20 Pandey C, Mahapatra M M, Kumar P & Giri A, *Met Mater Int*, 23 (2017) 900.
21 Pandey C, Mahapatra M M, Kumar P & Saini N, *J Press Vessel Technol*, 140 (2018) 214071.
22 Vishvesha A, Pandey C, Mahapatra M M & Mulik R S, *Int J Steel Struct*, 17 (2017) 53.
23 Kamble A G & Rao R V, *Indian J Eng Mater S*, 24 (2017) 413.
24 Shokri V, Sadeghi S, Sadeghi M H & Javadi Y, *J Non destruct Eval*, 34 (2015) 27.
25 Fu G, Lourenço M I, Duan M & Estefen S F, *Marine Struct,* 46 (2016) 30.
26 Fonda R W, Pao P S, Jones H N, Feng C R, Connolly B J & Davenport A J, *Mater Sci Eng A,* 519 (2009) 1.

27 *ASME Boiler and pressure vessel code: section II- part D properties* (ASME, New York), (2015).
28 *ASTM E 21–09: Standard test methods for elevated temperature tension tests of metallic materials* (ASTM International, New York), (2009).
29 Javadi Y, Smith M C, Abburi Vnkata K, Naveed N, Forsey A N & Francis J A, *et al.*, *Int J Pres Ves Pip*, 154 (2017) 41.
30 Rossini N S, Dassisti M, Benyounis K & Olabi A G, *Mater Des*, 35 (2011) 572.
31 Malik A, Qureshi E, Dar N & Khan I, *Thin Wall Struct,* 46 (2008) 1391.
32 Goldak J & Akhlaghi M, *Computational welding mechanics,* Springer (2005), ISBN: 978-0-387-23288-1.
33 DuPont J N & Marder A R, *Weld J,* 74 (1995) 406s.
34 Roy R K, *Design of experiments using the taguchi approach: 16 steps to product and process improvement ,* John Wiley & Sons (2001), ISBN: 978-0-471-36101-5.
35 Ghani JA, Jamaluddin H, Rahman M N & Deros B, *Asian J Sci Res,* 6 (2013) 27.
36 Meseguer-Valdenebro J, Portoles A & Oñoro J, *Indian J Eng Mater S*, 23 (2016) 341.